JCIM JOURNAL OF CHEMICAL INFORMATION AND MODELING

pubs.acs.org/jcim Article

The Leu/Val$^{6.51}$ Side Chain of Cannabinoid Receptors Regulates the Binding Mode of the Alkyl Chain of Δ^9-Tetrahydrocannabinol

Claudia Llinas del Torrent,[▽] Iu Raïch,[▽] Angel Gonzalez, Nil Casajuana-Martin, Jaume Lillo, Joan Biel Rebassa, Carlos Ferreiro-Vera, Verónica Sánchez de Medina, Rafael Franco, Gemma Navarro, and Leonardo Pardo*

Cite This: J. Chem. Inf. Model. 2023, 63, 5927−5935 Read Online

ACCESS | Metrics & More | Article Recommendations

ABSTRACT: (−)-Δ^9-*trans*-tetrahydrocannabinol (THC), which is the principal psychoactive constituent of *Cannabis*, mediates its action by binding to two members of the G-protein-coupled receptor (GPCR) family: the cannabinoid CB_1 (CB_1R) and CB_2 (CB_2R) receptors. Molecular dynamics simulations showed that the pentyl chain of THC could adopts an I-shape conformation, filling an intracellular cavity between Phe$^{3.36}$ and Trp$^{6.48}$ for initial agonist-induced receptor activation, in CB_1R but not in CB_2R. This cavity opens to the five-carbon chain of THC by the conformational change of the γ-branched, flexible, Leu$^{6.51}$ side chain of CB_1R, which is not feasible by the β-branched, mode rigid, Val$^{6.51}$ side chain of CB_2R. In agreement with our computational results, THC could not decrease the forskolin-induced cAMP levels in cells expressing mutant $CB_1R^{L6.51V}$ receptor but could activate the mutant $CB_2R^{V6.51L}$ receptor as efficiently as wild-type CB_1R. Additionally, JWH-133, a full CB_2R agonist, contains a branched dimethyl moiety in the ligand chain that bridges Phe$^{3.36}$ and Val$^{6.51}$ for receptor activation. In this case, the substitution of Val$^{6.51}$ to Leu in CB_2R makes JWH-133 unable to activate $CB_2R^{V6.51L}$. In conclusion, our combined computational and experimental results have shown that the amino acid at position 6.51 is a key additional player in the initial mechanism of activation of GPCRs that recognize signaling molecules derived from lipid species.

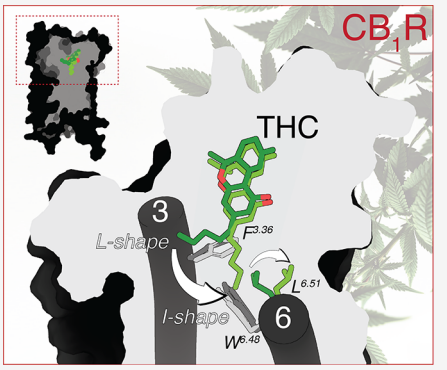

1. INTRODUCTION

Cannabinoids are naturally occurring compounds found in the *Cannabis sativa* plant (more commonly known as marijuana). There are over 180 cannabinoids out of the 1600 chemical compounds that have been isolated from *Cannabis*, with a characteristic oxygen containing C_{21} aromatic hydrocarbons.[1] These exogenous cannabinoids can be further classified into 11 subclasses: cannabichromene (CBC), cannabidiol (CBD), cannabielsoin (CBE), cannabigerol (CBG), cannabicyclol (CBL), cannabinol (CBN), cannabinodiol (CBND), cannabitriol (CBT), (−)-Δ^8-trans-tetrahydrocannabinol (Δ^8-THC), (−)-Δ^9-trans-tetrahydrocannabinol (Δ^9-THC), and miscellaneous-type cannabinoids.[2] The Δ^9-THC subclass contains 25 compounds with common structural features such as a dibenzopyran ring and a hydrophobic alkyl chain. This class includes the most abundant phytocannabinoids: (−)-Δ^9-*trans*-tetrahydrocannabinol (THC), which is the principal psychoactive constituent of *Cannabis*, and (−)-Δ^9-trans-tetrahydrocannabivarin (THCV), which is homologous to THC but has a 3-carbon (propyl chain) instead of a 5-carbon (pentyl chain) in the alkyl chain (Figure 1). THCV lacks the psychoactive effects of THC and upregulates energy metabolism, converting it a clinically useful remedy for weight loss, obesity management,

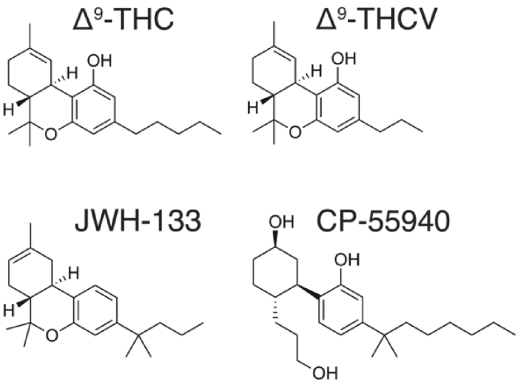

Figure 1. Structures of Δ^9-THC, Δ^9-THCV, JWH-133, and CP-55940.

Received: July 12, 2023
Published: August 30, 2023

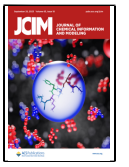

https://doi.org/10.1021/acs.jcim.3c01054
J. Chem. Inf. Model. 2023, 63, 5927−5935

and type 2 diabetic patients.[3,4] In addition, THCV can produce beneficial antipsychotic effects.[5] Endogenous cannabinoids are *N*-arachidonylethanolamide (anandamide) and 2-arachidonoylglycerol (2-AG) that possess long hydrophobic moieties.[6]

The effects of cannabinoids are primarily mediated through two members of the G-protein-coupled receptor (GPCR) family,[7] the cannabinoid CB_1 (CB_1R) and CB_2 (CB_2R) receptors. CB_1R is one of the most abundant GPCRs in the central nervous system, whereas CB_2R is mainly expressed in the immune system.[8] However, other molecular targets for certain cannabinoids, aside from CB_1R and CB_2R, have also been identified.[9] Some authors propose that THCV is a CB_1R and CB_2R antagonist,[10] whereas others suggest that THC and THCV are partial agonists at both receptors.[11] We have recently shown that THC acts as a partial agonist in CB_1R and as an antagonist in CB_2R, whereas THCV acts as an antagonist on both receptors.[12]

Here, we have used the recently released structures of CB_1R[13−15] and CB_2R[16−18] in their inactive and active, G_i-bound, conformations to delineate the individual signaling contributions of THC and THCV to modulate both receptors. $Phe^{3.36}$ and $Trp^{6.48}$ have been described as conformational toggle or trigger switches involved in the initial agonist-induced receptor activation in CB_1R,[15,19] CB_2R[16] and other GPCRs.[20−22] However, these amino acids are conserved in CB_1R and CB_2R (44% sequence identity between receptors), thus they cannot explain the different pharmacological profile of THC and THCV. In this manuscript, a combination of molecular dynamics (MD) simulations and site-directed mutagenesis have permitted to propose residue at position 6.51, which is Leu at CB_1R and Val at CB_2R, as an additional player capable to selectively recognize the alkyl chain of these ligands, further supporting the yin-yang functional relationship already described for CB_1 and CB_2 receptors.[16] This knowledge could be of great use to facilitate the future design of selective drugs in the endocannabinoid system.

2. MATERIALS AND METHODS

2.1. Initial CB_1R and CB_2R Models. The CB_1R-AM841-G_i (PDB id 6KPG) and CB_2R-AM12033-G_i (6KPF) cryo-EM structures[18] were used in docking studies and MD simulations. Missing residues 55−180 of α_i in the CB_1R-AM841-G_i structure were built from the structure of G_i (6CRK);[23] and missing residues 55−181 and 233−239 of α_i in the CB_2R-AM12033-G_i structure were built from the CB_2R-WIN55,212−2-G_i structure (6PT0),[17] using AutoModel class[24] of MODELER v10.1.[25] Protonation states were assigned with the PDB 2PQR tool[26] using PROPKA to predict the pK_a values of ionizable groups in the proteins at pH 6.5.[27] Disulfide bonds between cysteines were built using the tleap module of Ambertools19. Internal water molecules were added to CB_1R and CB_2R using HomolWat.[28] THC and THCV were docked into the orthosteric binding cavity of CB_1R and CB_2R and JWH-133 into CB_2R by using AM841 in 6KPG and AM12033 in 6KPF structures as a reference. Thus, the alkyl chains of THC, THCV, and JWH-133 were initially modeled in the L-shape conformation above $Trp279^{5.43}$ and $Trp194^{5.43}$ of CB_1R and CB_2R, respectively, as observed in the cryo-EM structures. These systems were oriented by the Orientations of Proteins in Membranes (OPM) database,[29] and embedded in a lipid bilayer box, constructed using PACKMOL-memgen,[30] containing 1-palmitoyl-2-oleoyl-*sn*-glycero-3-phosphocholine (POPC), cholesterol (CHL) (10:1 POPC:CHL ratio), water molecules (TIP3P), and monatomic Na^+ and Cl^- ions (0.15 M). The resulting systems comprise between 225 and 250k atoms in a box of ∼120 Å × 120 Å × 140 Å (see the Supporting Information in the Zenodo repository for detailed values).

2.2. Molecular Dynamics Simulations. MD simulations of these models were performed with GROMACS2018.5.[31] The amber14sb-ildn force field was used for the protein, solvent, and ions,[32] a GROMACS adaptation of lipid14 for lipids,[33] and the general Amber force field (GAFF2) with HF/6-31G*-derived RESP atomic charges for THC, THCV, and JWH-133.[34] Molecular systems were subjected to 5000 steps of energy minimization, using the steepest descent algorithm, PME electrostatics, with the Verlet cutoff scheme. This was followed by a 25 ns equilibration protocol consisting of six steps, in which positional restraints are progressively removed, from all heavy atoms to only helix Cα carbons being restricted, meanwhile gradually reducing the applied forces, from 1000 kJ mol^{-1} nm^{-2} to 0 kJ mol^{-1} nm^{-2}. After equilibration, three replicas of a 1 μs unrestrained MD trajectory were generated at a constant temperature of 300 K using separate v-rescale thermostats for the receptor, ligand, lipids, and solvent molecules. Initial velocities were randomly generated for each replica from a Maxwell distribution, using different random seeds. A time step of 2.0 fs was used for the integration of equations of motions using the leapfrog algorithm. Bonds involving hydrogen atoms were kept frozen by using the LINCS algorithm. Lennard-Jones interactions were computed using a cutoff of 1.1 nm under the Verlet cutoff scheme for neighbor searching, and the electrostatic interactions were treated using PME with the same real-space cutoff under periodic boundary conditions. Center of mass motion was removed from all systems. The Berendsen pressure control algorithm was chosen for equilibration and Parrinello−Rahman for production MDs. For complete details, see the Supporting Information in the Zenodo repository.

2.3. MD Analysis and Data Visualization. The analysis of the trajectories was performed using MDAnalysis;[35] visualization and image rendering were performed with PyMOL[36] and VMD,[37] and graphical representations were obtained with the Seaborn Package.[38]

2.4. CB_1R and CB_2R Mutants. Mutations were produced using the QuikChange Site-Directed Mutagenesis Kit. The cDNA for hCB_1R and hCB_2R, cloned into pcDNA3.1, was amplified using sense and antisense primers harboring the triplets for the desired point mutation (Pfu turbo polymerase was used). The nonmutated DNA template was digested for 1 h with DpnI. PCR products were used to transform XL1-blue supercompetent cells. Finally, positive colonies were tested by sequencing to select those expressing the correct DNA sequence.

2.5. cAMP Determination Assays. Determination of cAMP levels in HEK-293T cells transiently expressing CB_1R or CB_2R (1 μg of cDNA) or the mutant version of the receptor was performed by using the Lance-Ultra cAMP kit (PerkinElmer). Two hours before initiating the experiment, the medium was substituted by a serum-free medium. Then, transfected cells were dispensed in white 384-well microplates at a density of 4000 cells per well and incubated for 15 min at room temperature with compounds, followed by 15 min incubation with forskolin, and 1 h more with homogeneous time-resolved fluorescence (HTRF) assay reagents. Fluorescence at 665 nm was analyzed on a PHERAstar Flagship

https://doi.org/10.1021/acs.jcim.3c01054
J. Chem. Inf. Model. 2023, 63, 5927−5935

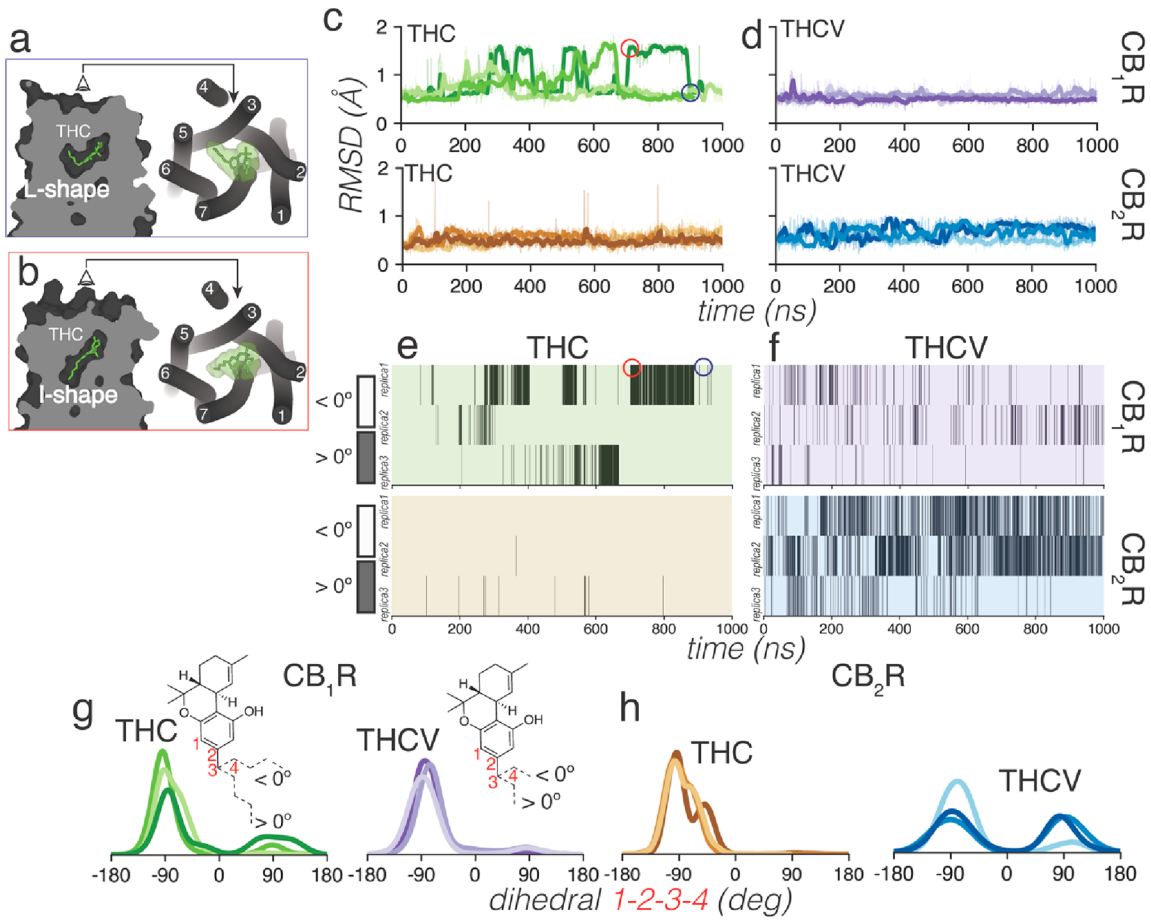

Figure 2. Conformational analysis of the alkyl chain of THC and THCV bound to CB_1R and CB_2R. Views parallel and perpendicular to the membrane plane of THC bound to CB_1R in (a) an L-shape and (b) an I-shape conformation pointing toward cavities between either TMs 3 and 5 or TMs 3 and 6, respectively. Red and blue rectangles correspond to the structure in red and blue circles in panels (c) and (e). Rmsd values of ligand heavy atoms (c, d), heatmaps (e, f) showing the conformation of the alkyl chain (dihedral angle 1−2−3−4) in the − *anticlinal* (angle around −90° < 0°) or the + *anticlinal* (around 90° > 0°), and histogram distribution of the dihedral angle 1−2−3−4 (g, h) during MD simulations of THC bound to CB_1R (green lines or panels) or CB_2R (brown) and THCV bound to CB_1R (purple) or CB_2R (blue). Three replicas of 1 μs of each complex were run.

microplate reader equipped with an HTRF optical module (BMG Labtech). Data analysis was made based on the fluorescence ratio emitted by the labeled cAMP probe (665 nm) over the light emitted by the europium cryptate-labeled anti-cAMP antibody (620 nm). A standard curve was used to calculate cAMP concentration. Forskolin-stimulated cAMP levels were normalized to 100%.

2.6. Pure Cannabinoids. Δ^9-THC and Δ^9-THCV substances were provided by Phytoplant Research S.L.U. Δ^9-THC and Δ^9-THCV were purified from the Moniek (CPVO/20160114) and Raquel (CPVO/20180114) varieties, respectively, using countercurrent chromatography as previously described.[39] The purity of both cannabinoids was set at >95%.

3. RESULTS

3.1. THC Adopts Two Distinct Binding Modes in CB_1R But Not in CB_2R. To understand the different molecular signatures of THC and THCV, at CB_1R and CB_2R, we first performed three replicate runs of unbiased 1 μs MD simulations of these compounds bound to the CB_1R-G_i and CB_2R-G_i complexes (see the Methods section). We have used G_i-bound active states, instead of inactive structures, despite its higher computational cost, because agonists alone are not capable to stabilize the fully active conformation in the absence of the G protein, as shown by NMR experiments.[40] Similarly, MD simulations of agonist bound to the inactive state of the receptor are not capable of reaching active-like conformations in the absence of the G protein. Moreover, MD simulations of active, G protein-bound, conformations have permitted to identify additional cavities to accommodate hydrophobic chains of ligands in sphingosine-1-phosphate[41] and muscarinic[42] receptors, which were not identified in similar simulations of inactive structures.

THC and THCV were docked into these structures with the hydrophobic alkyl tail in the L-shape conformation, as observed in the cryo-EM structures of structurally similar ligands (see the Methods section). Root-mean-square deviations (rmsd) of the ligand heavy atoms show that THC visited during the MD simulations two different poses in the binding pocket of CB_1R but not in CB_2R (Figure 2c). In CB_1R, THC adopts the initial L-shape conformation, in which the hydrophobic alkyl tail occupies a cavity between TMs 3 and 5 (Figure 2a), and an I-shape conformation, in which the alkyl tail occupies an intracellular cavity between TMs 3 and 6 (Figure 2b). The structure−function of the alkyl chain of THC has been reviewed,[43] and this dual orientation is consistent with previous studies by others.[15,44] The different conforma-

https://doi.org/10.1021/acs.jcim.3c01054
J. Chem. Inf. Model. 2023, 63, 5927−5935

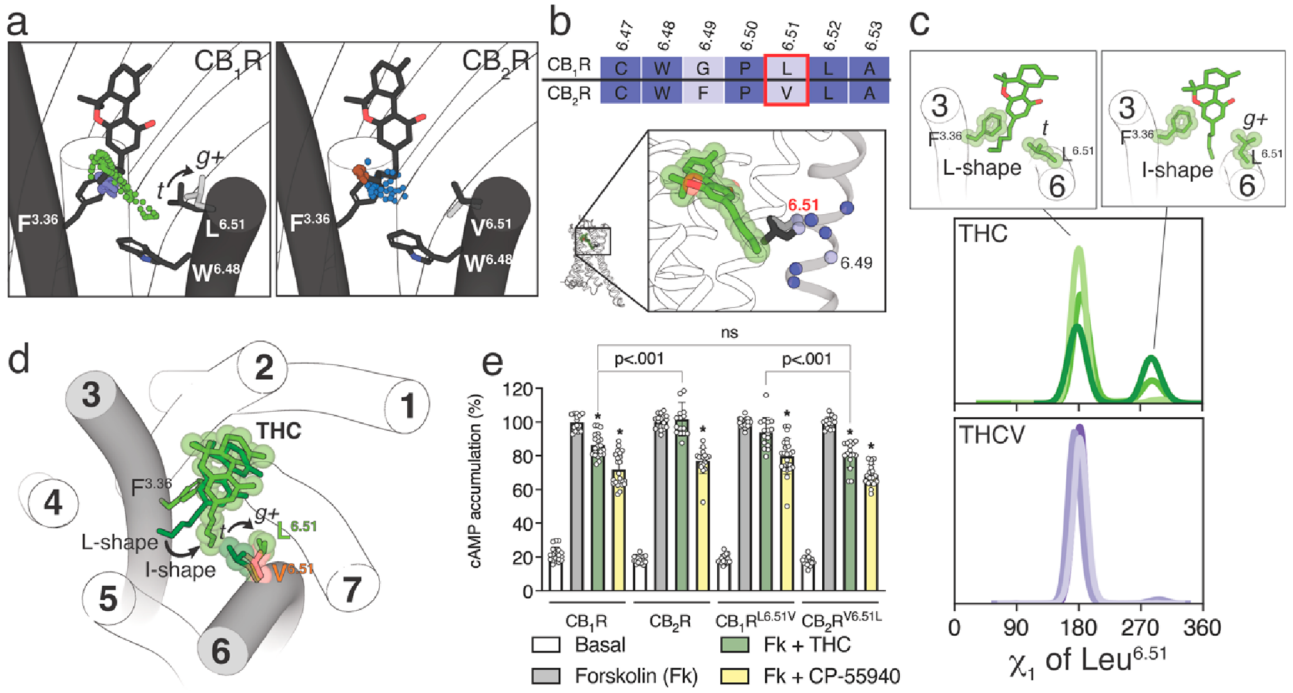

Figure 3. Conformational analysis of the Leu/Val$^{6.51}$ side chains of CB_1R and CB_2R. (a) Evolution of the terminal methyl group (color spheres) of the alkyl chain of THC or THCV during MD simulations of THC bound to CB_1R (green) or CB_2R (brown) and THCV bound to CB_1R (purple) or CB_2R (blue). The black arrow represents the conformational change of the side chain of Leu$^{6.51}$ from *t* to *g*+ that is triggered by the I-shaped conformation of THC in CB_1R. (b) Sequence comparison of TM 6 between CB_1R and CB_2R and the position of these amino acids in CB_1R (THC in the I-shaped conformation is shown as a reference). (c) Histogram distributions of the χ_1 dihedral angle of Leu$^{6.51}$ along the MD simulations of CB_1R bound to THC or THCV. Leu$^{6.51}$ adopted the *t* conformation with THCV and visited both the *t* and *g*+ conformations with THC. Representative structures of these conformations are also shown on the top panels. (d) Molecular representation of the different conformations of the five-carbon pentyl chain of THC (L- and I-shape) and Leu$^{6.51}$ in CB_1R (*t* and *g*+). The transition of the alkyl chain of THC from the L-shape to the I-shape conformation (black arrow), to fill the intracellular cavity between TMs 3 and 6 delineated by Phe$^{3.36}$, Trp$^{6.48}$, and Leu$^{6.51}$, requires the conformational transition of Leu$^{6.51}$ from *t* to *g*+ (black arrow). THC in the I-shape conformation and Leu$^{6.51}$ are shown in VdW spheres to visualize the narrow size of the intracellular cavity. Val$^{6.51}$ of CB_2R (in orange) is superimposed to perceive that the β-branched character of the side chain blocks the access of the ligand chain to the intracellular cavity. (e) CAMP levels determined in HEK-293T cells transfected with CB_1R, CB_2R, $CB_1R^{L6.51V}$, or $CB_2R^{V6.51L}$. Cells were pretreated with vehicle (basal) or with THC (10 μM) or CP-55940 (100 nM) upon exposure to forskolin (Fk, 500 nM). Values are means ± SD (n = 4 with sixtiplicates in all experiments) of the percentage of forskolin-induced cAMP formation. These values were analyzed statistically with one-way ANOVA, followed by Bonferroni's multiple comparison test (*: $p < 0.05$ compared with Fk).

tion of the pentyl chain of THC is achieved by a change of a single dihedral angle in the chain, from − *anticlinal* (dihedral 1−2−3−4 around −90°) in the L-shape to + *anticlinal* (around 90°) in the I-shape (Figure 2g). Heatmaps showing when THC adopts the − *anticlinal* (dihedral <0°) or + *anticlinal* (>0°) conformation correlates with large (I-shape) and small (L-shape) rmsd values, respectively (Figures 2c and 2e). Notably, the pentyl chain of THC in CB_2R rarely adopts the + *anticlinal* conformation (Figure 2e), thus no large rmsd values could be observed from the initial L-shape conformation during the MD simulations (Figure 2c). The shorter 3-carbon propyl chain of THCV has fewer steric constraints and can visit the + *anticlinal* conformation in both CB_1R and CB_2R simulations (Figures 2f−h).

It is not clear why the five-carbon pentyl chain of THC can also adopt the I-shape conformation, in which the alkyl tail occupies an intracellular cavity between TMs 3 and 6, in CB_1R but not in CB_2R. This intracellular cavity is delineated by the amino acid at position 6.51 (Figure 3a), which is Leu at CB_1R and Val at CB_2R (Figure 3b). The probability to undergo a side chain conformational change in Val is smaller than in Leu,[45] due to the β-branched side chain that is shorter than the γ-branched side chain of Leu. Val is generally found with the γ-carbons flanking the small Hα in the *trans* (*t*, χ_1 = 180°) rotamer conformation, whereas Leu can adopt the more stable *trans* (*t*, χ_1 = 180°) and less stable *gauche*+ (*g*+, χ_1 = −60°) rotamer conformations, as observed in the dynameomics rotamer library.[46] Figure 3c shows the histogram distributions of the χ_1 dihedral angle of Leu$^{6.51}$ along the MD simulations of CB_1R. These panels illustrate that the three-carbon propyl chain of THCV maintains Leu$^{6.51}$ in the more stable *t* conformation during the simulation time, whereas the five-carbon pentyl chain of THC in the I-shape conformation triggers or stabilizes the *g*+ conformation of Leu$^{6.51}$ in CB_1R, opening the access to the intracellular cavity between TMs 3 and 6 (Figure 3d). In contrast, the conformation of the bulky, β-branched, and more rigid side chain of Val$^{6.51}$ in CB_2R cannot be modified by the pentyl chain of THC (not shown), closing the access to the intracellular cavity.

3.2. The $CB_1R^{L6.51V}$ and $CB_2R^{V6.51L}$ Mutations Reverse the Pharmacology of THC. To experimentally validate the proposed different conformations of THC in CB_1R and CB_2R, we mutated Leu$^{6.51}$ to Val in CB_1R ($CB_1R^{L6.51V}$) and Val$^{6.51}$ to Leu in CB_2R ($CB_2R^{V6.51L}$), and we measured cAMP production in HEK-293T cells (Figure 3e). The nonselective CP-55940 agonist (100 nM) decreased, as expected for a G_i-coupled receptor, cAMP formation induced by forskolin (500 nM), in a statistically significant manner, in wild-type CB_1R

https://doi.org/10.1021/acs.jcim.3c01054
J. Chem. Inf. Model. 2023, 63, 5927−5935

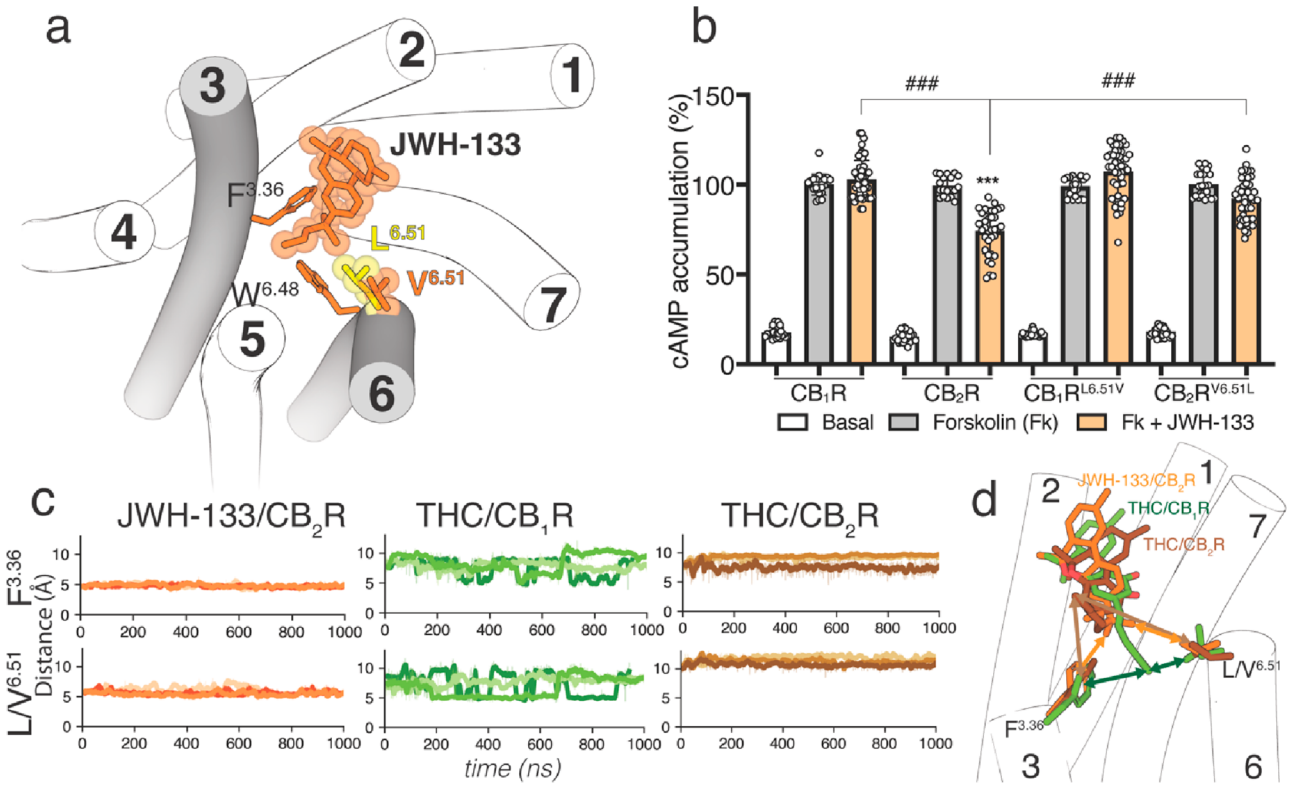

Figure 4. (a) The binding of JWH-133 to CB_2R. $Leu^{6.51}$ of CB_1R (in yellow) is superimposed to perceive the longer side chain of Leu in *t* compared to Val. (b) cAMP levels determined in HEK-293T cells transfected with CB_1R, CB_2R, $CB_1R^{L6.51V}$, or $CB_2R^{V6.51L}$. Cells were pretreated with vehicle (basal) or with JWH-133 (100 nM) upon exposure to forskolin (Fk, 500 nM). Values are means ± SD ($n = 4$ with sixtiplicates in all experiments) of the percentage of forskolin-induced cAMP formation. These values were analyzed statistically with two-way ANOVA, followed by Bonferroni's multiple comparison test ((***) $p < 0.001$ compared with Fk, (###) $p < 0.001$). (c) Distances between the terminal methyl group of the alkyl chain of THC and the dimethyl moiety of the dimethylbutyl chain of JWH-133 and the centroid of the aromatic ring of $Phe^{3.36}$ and either the δ- or γ- carbon of Leu/$Val^{6.51}$ of CB_1R or CB_2R (matching color arrows in panel (d) obtained during three replicas of MD simulations. (d) Comparison of the proposed binding modes of JWH-133 and THC in CB_2R and THC in CB_1R.

and CB_2R and mutant $CB_1R^{L6.51V}$ and $CB_2R^{V6.51L}$. In contrast, THC (10 μM) can significantly decrease forskolin-induced cAMP accumulation in CB_1R but not in CB_2R. We used high concentrations of THC to evaluate the greatest attainable response (ceiling effect). These results suggest that, in cAMP measurements, THC acts as a weak partial agonist only in CB_1R. Remarkably, the pharmacological profile of THC changes in the mutant receptors. THC can significantly decrease forskolin-induced cAMP accumulation in $CB_2R^{V6.51L}$ but not in $CB_1R^{L6.51V}$. Moreover, cAMP accumulation induced by THC is not statistically different between CB_1R and $CB_2R^{V6.51L}$. These experimental results, together with computational simulations, suggest that the residue at position 6.51, which is Leu at CB_1R and Val at CB_2R, is an additional element in the mechanism of receptor activation (see the Discussion section).

3.3. JWH-133 Activates CB_2R via the Substituted Methyl Groups. JWH-133 is a potent CB_2R agonist, with little affinity for CB_1R.[47] The structure of JWH-133 is like THC and THCV with a 4-carbon butyl chain, instead of the 3-carbon propyl chain of THCV or the 5-carbon pentyl chain of THC (Figure 1). A significant difference between JWH-133 and either THC or THCV is the methyl substitutions on the chain (Figure 1). Branching close to the aromatic ring might restrict the dimethylbutyl chain conformation of JWH-133. Thus, it seems reasonable to study the molecular properties of JWH-133, as a full agonist, in complex with CB_2R-G_i to challenge our proposed molecular models of THC and THCV (see section 3.1). Consequently, we performed simulations similar to those with THC and THCV to evaluate the binding mode of JWH-133 in CB_2R (see the Methods section). The alkyl chain of JWH-133 always adopts the L-shape conformation in the + *anticlinal* conformation, filling the cavity between TMs 3 and 5 (Figure 4a). The dimethyl moiety of the dimethylbutyl chain mediates hydrophobic interactions with $Phe^{3.36}$ and $Val^{6.51}$, during the simulation time (Figure 4c). To experimentally validate the key role of $Val^{6.51}$ in JWH-133-induced CB_2R activation, we measured the level of production of cAMP in $CB_1R^{L6.51V}$ and $CB_2R^{V6.51L}$ mutant receptors expressed in HEK-293T cells (Figure 4b). JWH-133 (100 nM) was unable to decrease forskolin-induced cAMP formation in CB_1R but was statistically significantly lower in CB_2R, as expected for a CB_2R selective agonist. Substitution of $Leu^{6.51}$ with Val in CB_1R does not facilitate activation of $CB_1R^{L6.51V}$ by JWH-133. However, substitution of the single $Val^{6.51}$ amino acid with Leu in CB_2R makes JWH-133 unable to activate $CB_2R^{V6.51L}$. This points to both the bulky, β-branched, and rigid $Val^{6.51}$ in CB_2R and the bulky, branched dimethyl group of the dimethylbutyl chain of JWH-133 as key elements for CB_2R activation (see the Discussion section). It was recently shown that the $CB_2R^{V6.51L}$ mutation also impeded HU308 and CP-55940, both containing the branched dimethyl group in the alkyl chain, to activate the G protein at CB_2R.[48]

https://doi.org/10.1021/acs.jcim.3c01054
J. Chem. Inf. Model. 2023, 63, 5927−5935

4. DISCUSSION AND CONCLUSIONS

Among the ~350 GPCRs for nonsensory functions, ~35 are activated by hormone-like signaling molecules derived from lipid species with long hydrophobic chains.[6,49] Some of these receptors possess distinctive structural signatures relative to other class A GPCRs such as the N-terminus and ECL-2 folding over the binding site,[50,51] which causes the entry of the ligand to the orthosteric site through a tunnel formed between TMs 1 and 7;[52,53] or lacking the highly conserved Pro$^{5.50}$, part of the PIF motif that transmits the signal from the orthosteric ligand binding site to the G protein binding site.[54,55] In PIF-containing GPCRs, the interaction of agonists with TM 5 triggers an inward movement of TM 5 at P$^{5.50}$, a rotation of TM 3 at I$^{3.40}$, and an outward movement of TM 6 at F$^{6.44}$.[56,57] In GPCRs lacking P$^{5.50}$, agonists can alter the rotamer of the amino acid at position 3.36[20] to trigger the rotation of TM 3 at I$^{3.40}$ and outward movement of TM 6 at F$^{6.44}$.[41] For instance, in the active crystal structure of S1P$_3$ bound to the endogenous agonist sphingosine-1-phosphate (S1P),[58] the long hydrophobic side chain of d18:1 S1P binds in an extended conformation (I-shape) between TMs 4 and 5 (Figure 5a).

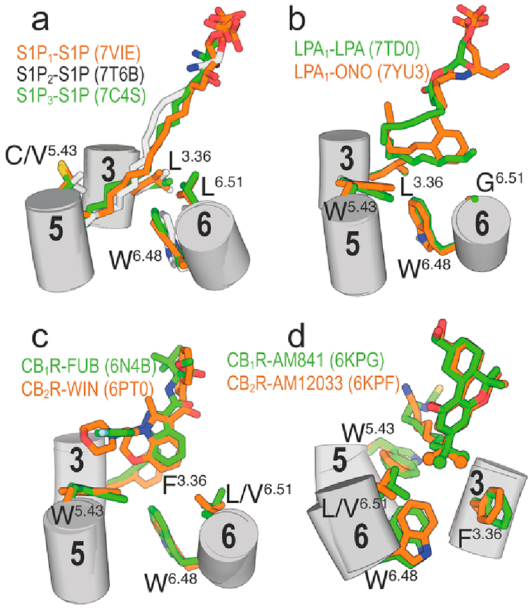

Figure 5. Cryo-EM structures of active S1P$_1$, S1P$_2$, or S1P$_3$ bound to S1P (a); active LPA$_1$ bound to LPA and ONO-0740556 (ONO) (b); active CB$_1$R bound to MDMB-Fubinaca (FUB) (c) and AM841 (d); and active CB$_2$R bound to WIN 55,212−2 (WIN) (c) and AM12033 (d). The branched dimethyl groups of AM841 and AM12033 are shown as spheres. Only key side chains at positions 3.36, 5.43, 6.48, and 6.51 are shown.

S1P triggers conformational changes of Leu122$^{3.36}$ from *t* to *g*+, among others (see quartet core in[58]), to accommodate the alkyl chain. Similar results were observed in S1P bound to S1P$_1$[59] and S1P$_2$[60] (Figure 5a). In the cryo-EM structure of active LPA$_1$ bound to the lysophosphatidic acid (LPA),[61] the alkyl chain of LPA cannot extend to the cleft between TMs 4 and 5 as S1P, due to the presence of the bulky Trp210$^{5.43}$ in LPA$_1$ (S1P$_{1-3}$ possess the less bulky Cys206$^{5.43}$, Val194$^{5.43}$, or Cys200$^{5.43}$), blocking the access. LPA adopts an U-shaped conformation bending backward and triggering the *g*+ conformation of Leu132$^{3.36}$ (Figure 5b). The long acyl chain of the ONO-0740556 agonist, a more rigid and potent LPA analog, binds LPA$_1$ in a different bent conformation than LPA[62] (Figure 5c). In this case, the aromatic ring of ONO-0740556 triggers the *g*+ conformation of Leu132$^{3.36}$. The lack of side chain in Gly274$^{6.51}$ (LPA$_{1-3}$ possess Gly at this key position) permits LPA$_1$ to have a small pocket in front of Leu132$^{3.36}$ encaging the terminus of LPA or the phenyl ring of ONO-0740556.[61,62]

CB$_1$R and CB$_2$R possess Trp279$^{5.43}$ and Trp194$^{5.43}$, respectively, thus blocking the TMs 4 and 5 cleft created in S1P binding to S1P$_{1-3}$; and contain Phe200$^{3.36}$ and Phe117$^{3.36}$, respectively, as conformational toggle or trigger switch involved in the initial agonist-induced receptor activation. Notably, the indazole ring of MDMB-Fubinaca triggers the active *g*+ conformation of Phe200$^{3.36}$ in CB$_1$R by an aromatic−aromatic interaction (Figure 5c),[15] and the aromatic core of WIN 55,212−2 also forms aromatic−aromatic interactions with Phe117$^{3.36}$ in *g*+ of CB$_2$R (Figure 5c).[17] In other known structures of active CB$_1$R and CB$_2$R bound to agonists, the bulky and branched dimethyl groups of the alkyl chain of AM841 and AM12033 bridge Phe200$^{3.36}$ in *g*+ and Leu359$^{6.51}$ of CB$_1$R and Phe117$^{3.36}$ in *g*+ and Val261$^{6.51}$ of CB$_2$R (Figure 5d), respectively.[18] The conformational change in Phe$^{3.36}$, from pointing toward TM 6 in *t* to pointing toward TM 7 in *g*+, permits Trp$^{6.48}$ to move toward TM 5 for receptor activation.

These data indicate that the hydrophobic alkyl chain of the signaling molecule is key in the process of ligand-induced receptor activation. Thus, in this paper, we have studied the conformation of the alkyl chain of THC, THCV, and JWH-133 bound to CB$_1$R and CB$_2$R and calculated their distances to Phe$^{3.36}$ along the MD simulations. Among them, the distances between the terminal methyl group of the alkyl chain of THC and the centroid of the aromatic ring of Phe$^{3.36}$ and either the *δ*- or *γ*- carbon of Leu/Val$^{6.51}$ are important to highlight (see Figures 4c and 4d). They fluctuated from >5 Å to <5 Å in CB$_1$R and are always >5 Å in CB$_2$R, indicating a dual orientation of the alkyl chain in CB$_1$R, which either occupies a cavity above Trp$^{5.43}$ (between TMs 3 and 5) in an L-shape conformation, or an intracellular cavity between Phe$^{3.36}$ and Trp$^{6.48}$ (TMs 3 and 6) in an I-shape conformation (Figure 3d). The main achievement of this work is the discovery that THC in CB$_1$R, but not in CB$_2$R, can adopt this I-shape conformation. The intracellular cavity between Phe$^{3.36}$ and Trp$^{6.48}$ is also delineated by the amino acid at position 6.51, which is the *γ*-branched, flexible Leu side chain in CB$_1$R and the *β*-branched, model rigid Val side chain in CB$_2$R (Figure 3b). We have shown that the five-carbon pentyl chain of THC can trigger the conformational change of Leu$^{6.51}$ from *t*, blocking the access of the chain to the intracellular cavity, to *g*+, opening the access (Figures 3c and 3d). This opening of the chain access to the intracellular cavity is not feasible with the rigid Val$^{6.51}$ side chain of CB$_2$R. The binding mode of THC in the I-shape conformation positions the alkyl chain between Phe$^{3.36}$ in the active *g*+ conformation and Trp$^{6.48}$ that is involved in the initial mechanism of agonist-induced receptor activation. Thus, these computational results are compatible with our experiments, showing that THC acts as a partial agonist in CB$_1$R and as an antagonist in CB$_2$R (Figure 3e).[12] In agreement with our computational results, THC could not activate the mutant CB$_1$R$^{L6.51V}$ receptor and activated the mutant CB$_2$R$^{V6.51L}$ receptor as efficiently as wild type CB$_1$R (Figure 3e). We have recently shown that the alkyl chain of cannabidiol, in the allosteric binding mode, also expands

https://doi.org/10.1021/acs.jcim.3c01054
J. Chem. Inf. Model. 2023, 63, 5927−5935

toward the intracellular cavity modulating the conformation of Phe$^{3.36}$.[63]

The predicted binding mode of the dimethylbutyl chain conformation of the full agonist JWH-133 at CB_2R is always in the L-shape conformation, filling the cavity between TMs 3 and 5 (Figure 4a). However, the branched dimethyl moiety of the ligand chain mediates hydrophobic interactions with Phe$^{3.36}$ in the active *g*+ conformation and Val$^{6.51}$ (Figure 4c). Notably, substitution of Val$^{6.51}$ for Leu in CB_2R makes JWH-133 unable to activate $CB_2R^{V6.51L}$ (Figure 4b). This supports the concept that the branched dimethylbutyl chain conformation of JWH-133 needs a foothold on the rigid Val$^{6.51}$ to move Phe$^{3.36}$ to the active *g*+ conformation for receptor activation.

In conclusion, our findings have shown that, in cannabinoid receptors and probably other receptors that recognize signaling molecules derived from lipid species with long hydrophobic chains, the amino acid at position 6.51 defines the size and shape of the cavity near Phe$^{3.36}$ and Trp$^{6.48}$ and is a key additional player in the mechanism of activation of this type of GPCRs.

■ ASSOCIATED CONTENT

Data Availability Statement

Input coordinates (.gro), topology files (.top), ligand parameters (.itp), input files, and representative structures collected during three replicas of MD simulations (in a PyMol session) of THC and THCV bound to CB_1R and CB_2R and JWH-133 bound to CB_2R (the color code of the structures is as given in Figures 2−4) are available at https://zenodo.org/record/8114762. PACKMOL-Memgen, distributed with AmberTools, is free of charge; the Seaborn Package, MDAnalysis and GROMACS are open source; VMD is available to noncommercial users under a distribution-specific license; and PyMOL is commercial software with paid license.

■ AUTHOR INFORMATION

Corresponding Author

Leonardo Pardo − *Laboratory of Computational Medicine, Biostatistics Unit, Faculty of Medicine, Universitat Autònoma Barcelona, 08193 Bellaterra, Barcelona, Spain;* orcid.org/0000-0003-1778-7420; Email: leonardo.pardo@uab.cat

Authors

Claudia Llinas del Torrent − *Laboratory of Computational Medicine, Biostatistics Unit, Faculty of Medicine, Universitat Autònoma Barcelona, 08193 Bellaterra, Barcelona, Spain*

Iu Raïch − *Department of Biochemistry and Molecular Biomedicine, School of Biology, University of Barcelona, 08028 Barcelona, Spain; Centro de Investigación en Red, Enfermedades Neurodegenerativas (CIBERNED), Instituto de Salud Carlos III, 28031 Madrid, Spain*

Angel Gonzalez − *Laboratory of Computational Medicine, Biostatistics Unit, Faculty of Medicine, Universitat Autònoma Barcelona, 08193 Bellaterra, Barcelona, Spain*

Nil Casajuana-Martin − *Laboratory of Computational Medicine, Biostatistics Unit, Faculty of Medicine, Universitat Autònoma Barcelona, 08193 Bellaterra, Barcelona, Spain*

Jaume Lillo − *Department of Biochemistry and Physiology, Faculty of Pharmacy and Food Sciences, Universitat de Barcelona, 08028 Barcelona, Spain*

Joan Biel Rebassa − *Department of Biochemistry and Physiology, Faculty of Pharmacy and Food Sciences, Universitat de Barcelona, 08028 Barcelona, Spain*

Carlos Ferreiro-Vera − *Phytoplant Research S.L.U., 14014 Córdoba, Spain*

Verónica Sánchez de Medina − *Phytoplant Research S.L.U., 14014 Córdoba, Spain*

Rafael Franco − *Department of Biochemistry and Molecular Biomedicine, School of Biology, University of Barcelona, 08028 Barcelona, Spain; Centro de Investigación en Red, Enfermedades Neurodegenerativas (CIBERNED), Instituto de Salud Carlos III, 28031 Madrid, Spain;* orcid.org/0000-0003-2549-4919

Gemma Navarro − *Centro de Investigación en Red, Enfermedades Neurodegenerativas (CIBERNED), Instituto de Salud Carlos III, 28031 Madrid, Spain; Department of Biochemistry and Physiology, Faculty of Pharmacy and Food Sciences, Universitat de Barcelona, 08028 Barcelona, Spain; Institute of Neuroscience, University of Barcelona (NeuroUB), 08028 Barcelona, Spain*

Complete contact information is available at: https://pubs.acs.org/10.1021/acs.jcim.3c01054

Author Contributions

[▽]These authors contributed equally. C.L.T. and I.R. devised the project concept and designed experiments. C.L.T., A.G., and N.C.-M. contributed with computational simulations. I.R., J.L., and J.B.R. performed biochemical assays. C.F.-V. and V.S.M. provided reagents. R.F., G.N., and L.P. supervised the project. L.P. wrote the paper with contributions from all other authors. All authors contributed to the data analysis and have given approval to the final version of the manuscript.

Notes

The authors declare no competing financial interest.

■ ACKNOWLEDGMENTS

We acknowledge the financial support from the Spanish Ministry of Economy and Innovation with FEDER funds (Nos. PID2020-113430RB-I00, PID2021-126600OB-I00, PDC2022-133171-I00, PID2022-140912OB-I00) and Generalitat de Catalunya (No. 2021 SGR 00304). C.L.T. is recipient of a FPI fellowship (No. BES-2017-081872).

■ REFERENCES

(1) Tahir, M. N.; Shahbazi, F.; Rondeau-Gagne, S.; Trant, J. F. The biosynthesis of the cannabinoids. *J. Cannabis Res.* **2021**, *3* (1), 7.

(2) Radwan, M. M.; Chandra, S.; Gul, S.; ElSohly, M. A. Cannabinoids, Phenolics, Terpenes and Alkaloids of Cannabis. *Molecules* **2021**, *26* (9), 2774.

(3) Jadoon, K. A.; Ratcliffe, S. H.; Barrett, D. A.; Thomas, E. L.; Stott, C.; Bell, J. D.; O'Sullivan, S. E.; Tan, G. D. Efficacy and Safety of Cannabidiol and Tetrahydrocannabivarin on Glycemic and Lipid Parameters in Patients With Type 2 Diabetes: A Randomized, Double-Blind, Placebo-Controlled, Parallel Group Pilot Study. *Diabetes Care* **2016**, *39* (10), 1777−86.

(4) Abioye, A.; Ayodele, O.; Marinkovic, A.; Patidar, R.; Akinwekomi, A.; Sanyaolu, A. Delta9-Tetrahydrocannabivarin (THCV): a commentary on potential therapeutic benefit for the management of obesity and diabetes. *J. Cannabis Res.* **2020**, *2* (1), 6.

(5) Cascio, M. G.; Zamberletti, E.; Marini, P.; Parolaro, D.; Pertwee, R. G. The phytocannabinoid, Delta(9)-tetrahydrocannabivarin, can act through 5-HT(1)A receptors to produce antipsychotic effects. *Br. J. Pharmacol.* **2015**, *172* (5), 1305−18.

(6) Krishna Deepak, R. N. V.; Verma, R. K.; Hartono, Y. D.; Yew, W. S.; Fan, H. Recent Advances in Structure, Function, and Pharmacology of Class A Lipid GPCRs: Opportunities and Challenges for Drug Discovery. *Pharmaceuticals (Basel)* **2022**, *15* (1), 12.
(7) Ferre, S.; Ciruela, F.; Dessauer, C. W.; Gonzalez-Maeso, J.; Hebert, T. E.; Jockers, R.; Logothetis, D. E.; Pardo, L. G protein-coupled receptor-effector macromolecular membrane assemblies (GEMMAs). *Pharmacol. Ther.* **2022**, *231*, No. 107977.
(8) Parsons, L. H.; Hurd, Y. L. Endocannabinoid signalling in reward and addiction. *Nat. Rev. Neurosci.* **2015**, *16* (10), 579−94.
(9) Morales, P.; Hurst, D. P.; Reggio, P. H. Molecular Targets of the Phytocannabinoids: A Complex Picture. *Prog. Chem. Org. Nat. Prod.* **2017**, *103*, 103−131.
(10) Thomas, A.; Stevenson, L. A.; Wease, K. N.; Price, M. R.; Baillie, G.; Ross, R. A.; Pertwee, R. G. Evidence that the plant cannabinoid Delta9-tetrahydrocannabivarin is a cannabinoid CB1 and CB2 receptor antagonist. *Br. J. Pharmacol.* **2005**, *146* (7), 917−26.
(11) Zagzoog, A.; Mohamed, K. A.; Kim, H. J. J.; Kim, E. D.; Frank, C. S.; Black, T.; Jadhav, P. D.; Holbrook, L. A.; Laprairie, R. B. In vitro and in vivo pharmacological activity of minor cannabinoids isolated from Cannabis sativa. *Sci. Rep.* **2020**, *10* (1), 20405.
(12) Raich, I.; Rivas-Santisteban, R.; Lillo, A.; Lillo, J.; Reyes-Resina, I.; Nadal, X.; Ferreiro-Vera, C.; de Medina, V. S.; Majellaro, M.; Sotelo, E.; Navarro, G.; Franco, R. Similarities and differences upon binding of naturally occurring Delta(9)-tetrahydrocannabinol-derivatives to cannabinoid CB1 and CB2 receptors. *Pharmacol. Res.* **2021**, *174*, No. 105970.
(13) Shao, Z.; Yin, J.; Chapman, K.; Grzemska, M.; Clark, L.; Wang, J.; Rosenbaum, D. M. High-resolution crystal structure of the human CB1 cannabinoid receptor. *Nature* **2016**, *540* (7634), 602−606.
(14) Hua, T.; Vemuri, K.; Pu, M.; Qu, L.; Han, G. W.; Wu, Y.; Zhao, S.; Shui, W.; Li, S.; Korde, A.; Laprairie, R. B.; Stahl, E. L.; Ho, J. H.; Zvonok, N.; Zhou, H.; Kufareva, I.; Wu, B.; Zhao, Q.; Hanson, M. A.; Bohn, L. M.; Makriyannis, A.; Stevens, R. C.; Liu, Z. J. Crystal Structure of the Human Cannabinoid Receptor CB1. *Cell* **2016**, *167* (3), 750−762.
(15) Krishna Kumar, K.; Shalev-Benami, M.; Robertson, M. J.; Hu, H.; Banister, S. D.; Hollingsworth, S. A.; Latorraca, N. R.; Kato, H. E.; Hilger, D.; Maeda, S.; Weis, W. I.; Farrens, D. L.; Dror, R. O.; Malhotra, S. V.; Kobilka, B. K.; Skiniotis, G. Structure of a Signaling Cannabinoid Receptor 1-G Protein Complex. *Cell* **2019**, *176* (3), 448−458.
(16) Li, X.; Hua, T.; Vemuri, K.; Ho, J. H.; Wu, Y.; Wu, L.; Popov, P.; Benchama, O.; Zvonok, N.; Locke, K.; Qu, L.; Han, G. W.; Iyer, M. R.; Cinar, R.; Coffey, N. J.; Wang, J.; Wu, M.; Katritch, V.; Zhao, S.; Kunos, G.; Bohn, L. M.; Makriyannis, A.; Stevens, R. C.; Liu, Z. J. Crystal Structure of the Human Cannabinoid Receptor CB2. *Cell* **2019**, *176* (3), 459−467.
(17) Xing, C.; Zhuang, Y.; Xu, T. H.; Feng, Z.; Zhou, X. E.; Chen, M.; Wang, L.; Meng, X.; Xue, Y.; Wang, J.; Liu, H.; McGuire, T. F.; Zhao, G.; Melcher, K.; Zhang, C.; Xu, H. E.; Xie, X. Q. Cryo-EM Structure of the Human Cannabinoid Receptor CB2-Gi Signaling Complex. *Cell* **2020**, *180* (4), 645−654.
(18) Hua, T.; Li, X.; Wu, L.; Iliopoulos-Tsoutsouvas, C.; Wang, Y.; Wu, M.; Shen, L.; Johnston, C. A.; Nikas, S. P.; Song, F.; et al. Activation and Signaling Mechanism Revealed by Cannabinoid Receptor-Gi Complex Structures. *Cell* **2020**, *180* (4), 655−665.
(19) McAllister, S. D.; Hurst, D. P.; Barnett-Norris, J.; Lynch, D.; Reggio, P. H.; Abood, M. E. Structural mimicry in class A G protein-coupled receptor rotamer toggle switches: the importance of the F3.36(201)/W6.48(357) interaction in cannabinoid CB1 receptor activation. *J. Biol. Chem.* **2004**, *279* (46), 48024−37.
(20) Pellissier, L. P.; Sallander, J.; Campillo, M.; Gaven, F.; Queffeulou, E.; Pillot, M.; Dumuis, A.; Claeysen, S.; Bockaert, J.; Pardo, L. Conformational toggle switches implicated in basal constitutive and agonist-induced activated states of 5-hydroxytryptamine-4 receptors. *Mol. Pharmacol.* **2009**, *75* (4), 982−990.
(21) Navarro, G.; Gonzalez, A.; Campanacci, S.; Rivas-Santisteban, R.; Reyes-Resina, I.; Casajuana-Martin, N.; Cordomi, A.; Pardo, L.; Franco, R. Experimental and computational analysis of biased agonism on full-length and a C-terminally truncated adenosine A2A receptor. *Comput. Struct. Biotechnol. J.* **2020**, *18*, 2723−2732.
(22) Ersoy, B. A.; Pardo, L.; Zhang, S.; Thompson, D. A.; Millhauser, G.; Govaerts, C.; Vaisse, C. Mechanism of N-terminal modulation of activity at the melanocortin-4 receptor GPCR. *Nat. Chem. Biol.* **2012**, *8* (8), 725−30.
(23) Maeda, S.; Koehl, A.; Matile, H.; Hu, H.; Hilger, D.; Schertler, G. F. X.; Manglik, A.; Skiniotis, G.; Dawson, R. J. P.; Kobilka, B. K. Development of an antibody fragment that stabilizes GPCR/G-protein complexes. *Nat. Commun.* **2018**, *9* (1), 3712.
(24) Webb, B.; Sali, A. Comparative Protein Structure Modeling Using MODELLER. *Curr. Protoc. Bioinformatics* **2016**, *54*, 5.6.1−5.6.32.
(25) Marti-Renom, M. A.; Stuart, A. C.; Fiser, A.; Sanchez, R.; Melo, F.; Sali, A. Comparative protein structure modeling of genes and genomes. *Annu. Rev. Biophys. Biomol. Struct.* **2000**, *29*, 291−325.
(26) Dolinsky, T. J.; Nielsen, J. E.; McCammon, J. A.; Baker, N. A. PDB2PQR: an automated pipeline for the setup of Poisson-Boltzmann electrostatics calculations. *Nucleic Acids Res.* **2004**, *32* (Web Server issue), W665−W667.
(27) Sondergaard, C. R.; Olsson, M. H.; Rostkowski, M.; Jensen, J. H. Improved Treatment of Ligands and Coupling Effects in Empirical Calculation and Rationalization of pKa Values. *J. Chem. Theory Comput.* **2011**, *7* (7), 2284−95.
(28) Mayol, E.; Garcia-Recio, A.; Tiemann, J. K. S.; Hildebrand, P. W.; Guixa-Gonzalez, R.; Olivella, M.; Cordomi, A. HomolWat: a web server tool to incorporate 'homologous' water molecules into GPCR structures. *Nucleic Acids Res.* **2020**, *48* (W1), W54−W59.
(29) Lomize, M. A.; Pogozheva, I. D.; Joo, H.; Mosberg, H. I.; Lomize, A. L. OPM database and PPM web server: resources for positioning of proteins in membranes. *Nucleic Acids Res.* **2012**, *40* (D1), D370−D376.
(30) Schott-Verdugo, S.; Gohlke, H. PACKMOL-Memgen: A Simple-To-Use, Generalized Workflow for Membrane-Protein-Lipid-Bilayer System Building. *J. Chem. Inf. Model.* **2019**, *59* (6), 2522−2528.
(31) Abraham, M. J.; Murtola, T.; Schulz, R.; Pall, S.; Smith, J. C.; Hess, B.; Lindahl, E. GROMACS: High performance molecular simulations through multi-level parallelism from laptops to supercomputers. *SoftwareX* **2015**, *1−2*, 19−25.
(32) Maier, J. A.; Martinez, C.; Kasavajhala, K.; Wickstrom, L.; Hauser, K. E.; Simmerling, C. ff14SB: Improving the Accuracy of Protein Side Chain and Backbone Parameters from ff99SB. *J. Chem. Theory Comput.* **2015**, *11* (8), 3696−713.
(33) Dickson, C. J.; Madej, B. D.; Skjevik, A. A.; Betz, R. M.; Teigen, K.; Gould, I. R.; Walker, R. C. Lipid14: The Amber Lipid Force Field. *J. Chem. Theory Comput.* **2014**, *10* (2), 865−879.
(34) Wang, J.; Wolf, R. M.; Caldwell, J. W.; Kollman, P. A.; Case, D. A. Development and testing of a general amber force field. *J. Comput. Chem.* **2004**, *25* (9), 1157−74.
(35) Michaud-Agrawal, N.; Denning, E. J.; Woolf, T. B.; Beckstein, O. MDAnalysis: a toolkit for the analysis of molecular dynamics simulations. *J. Comput. Chem.* **2011**, *32* (10), 2319−27.
(36) *The PyMOL Molecular Graphics System*, Version 1.3r1; Schrodinger, LLC, 2010.
(37) Humphrey, W.; Dalke, A.; Schulten, K. VMD: visual molecular dynamics. *J. Mol. Graph.* **1996**, *14* (1), 33−8.
(38) Waskom, M. L. seaborn: statistical data visualization. *J. Open Source Softw.* **2021**, *6* (60), 3021.
(39) Nadal, X. Methods of purifying cannabinoids using liquid:liquid chromatography. US10207199B2, 2019.
(40) Nygaard, R.; Zou, Y.; Dror, R. O.; Mildorf, T. J.; Arlow, D. H.; Manglik, A.; Pan, A. C.; Liu, C. W.; Fung, J. J.; Bokoch, M. P.; Thian, F. S.; Kobilka, T. S.; Shaw, D. E.; Mueller, L.; Prosser, R. S.; Kobilka, B. K. The Dynamic Process of beta(2)-Adrenergic Receptor Activation. *Cell* **2013**, *152* (3), 532−42.

https://doi.org/10.1021/acs.jcim.3c01054
J. Chem. Inf. Model. 2023, 63, 5927−5935

(41) Troupiotis-Tsailaki, A.; Zachmann, J.; Gonzalez-Gil, I.; Gonzalez, A.; Ortega-Gutierrez, S.; Lopez-Rodriguez, M. L.; Pardo, L.; Govaerts, C. Ligand chain length drives activation of lipid G protein-coupled receptors. *Sci. Rep.* **2017**, *7* (1), 2020.
(42) Powers, A. S.; Pham, V.; Burger, W. A. C.; Thompson, G.; Laloudakis, Y.; Barnes, N. W.; Sexton, P. M.; Paul, S. M.; Christopoulos, A.; Thal, D. M.; Felder, C. C.; Valant, C.; Dror, R. O. Structural basis of efficacy-driven ligand selectivity at GPCRs. *Nat. Chem. Biol.* **2023**, *19*, 805.
(43) Bow, E. W.; Rimoldi, J. M. The Structure-Function Relationships of Classical Cannabinoids: CB1/CB2Modulation. *Perspect. Medicin. Chem.* **2016**, *8*, 17−39.
(44) Jung, S. W.; Cho, A. E.; Yu, W. Exploring the Ligand Efficacy of Cannabinoid Receptor 1 (CB1) using Molecular Dynamics Simulations. *Sci. Rep.* **2018**, *8* (1), 13787.
(45) Gaudreault, F.; Chartier, M.; Najmanovich, R. Side-chain rotamer changes upon ligand binding: common, crucial, correlate with entropy and rearrange hydrogen bonding. *Bioinformatics* **2012**, *28* (18), i423−i430.
(46) Scouras, A. D.; Daggett, V. The Dynameomics rotamer library: amino acid side chain conformations and dynamics from comprehensive molecular dynamics simulations in water. *Protein Sci.* **2011**, *20* (2), 341−52.
(47) Huffman, J. W.; Liddle, J.; Yu, S.; Aung, M. M.; Abood, M. E.; Wiley, J. L.; Martin, B. R. 3-(1′,1′-Dimethylbutyl)-1-deoxy-delta8-THC and related compounds: synthesis of selective ligands for the CB2 receptor. *Bioorg. Med. Chem. Lett.* **1999**, *7* (12), 2905−14.
(48) Li, X.; Chang, H.; Bouma, J.; de Paus, L. V.; Mukhopadhyay, P.; Paloczi, J.; Mustafa, M.; van der Horst, C.; Kumar, S. S.; Wu, L.; Yu, Y.; van den Berg, R.; Janssen, A. P. A.; Lichtman, A.; Liu, Z. J.; Pacher, P.; van der Stelt, M.; Heitman, L. H.; Hua, T. Structural basis of selective cannabinoid CB(2) receptor activation. *Nat. Commun.* **2023**, *14* (1), 1447.
(49) Alexander, S. P.; Christopoulos, A.; Davenport, A. P.; Kelly, E.; Marrion, N. V.; Peters, J. A.; Faccenda, E.; Harding, S. D.; Pawson, A. J.; Sharman, J. L.; Southan, C.; Davies, J. A. the Concise Guide to Pharmacology 2017/18: G protein-coupled receptors. *Br. J. Pharmacol.* **2017**, *174* (Suppl 1), S17−S129.
(50) Gonzalez, A.; Cordomí, A.; Caltabiano, G.; Pardo, L. Impact of helix irregularities on sequence alignment and homology modelling of G protein-coupled receptors. *Chembiochem* **2012**, *13* (10), 1393−1399.
(51) Audet, M.; Stevens, R. C. Emerging structural biology of lipid G protein-coupled receptors. *Protein Sci.* **2019**, *28* (2), 292−304.
(52) Stanley, N.; Pardo, L.; Fabritiis, G. D. The pathway of ligand entry from the membrane bilayer to a lipid G protein-coupled receptor. *Sci. Rep.* **2016**, *6*, 22639.
(53) Casajuana-Martin, N.; Navarro, G.; Gonzalez, A.; Llinas Del Torrent, C.; Gomez-Autet, M.; Quintana Garcia, A.; Franco, R.; Pardo, L. A Single Point Mutation Blocks the Entrance of Ligands to the Cannabinoid CB(2) Receptor via the Lipid Bilayer. *J. Chem. Inf. Model.* **2022**, *62* (22), 5771−5779.
(54) Weis, W. I.; Kobilka, B. K. The Molecular Basis of G Protein-Coupled Receptor Activation. *Annu. Rev. Biochem.* **2018**, *87*, 897−919.
(55) Zhou, Q.; Yang, D.; Wu, M.; Guo, Y.; Guo, W.; Zhong, L.; Cai, X.; Dai, A.; Jang, W.; Shakhnovich, E. I.et al. Common activation mechanism of class A GPCRs. *Elife* **2019**, *8*, DOI: 10.7554/eLife.50279.
(56) Sansuk, K.; Deupi, X.; Torrecillas, I. R.; Jongejan, A.; Nijmeijer, S.; Bakker, R. A.; Pardo, L.; Leurs, R. A Structural Insight into the Reorientation of Transmembrane Domains 3 and 5 during Family A G Protein-Coupled Receptor Activation. *Mol. Pharmacol.* **2011**, *79* (2), 262−9.
(57) Rasmussen, S. G.; Choi, H. J.; Fung, J. J.; Pardon, E.; Casarosa, P.; Chae, P. S.; Devree, B. T.; Rosenbaum, D. M.; Thian, F. S.; Kobilka, T. S.; Schnapp, A.; Konetzki, I.; Sunahara, R. K.; Gellman, S. H.; Pautsch, A.; Steyaert, J.; Weis, W. I.; Kobilka, B. K. Structure of a nanobody-stabilized active state of the beta(2) adrenoceptor. *Nature* **2011**, *469* (7329), 175−80.
(58) Maeda, S.; Shiimura, Y.; Asada, H.; Hirata, K.; Luo, F.; Nango, E.; Tanaka, N.; Toyomoto, M.; Inoue, A.; Aoki, J.; Iwata, S.; Hagiwara, M. Endogenous agonist-bound S1PR3 structure reveals determinants of G protein-subtype bias. *Sci. Adv.* **2021**, *7* (24), DOI: 10.1126/sciadv.abf5325.
(59) Yu, L.; He, L.; Gan, B.; Ti, R.; Xiao, Q.; Yang, X.; Hu, H.; Zhu, L.; Wang, S.; Ren, R. Structural insights into sphingosine-1-phosphate receptor activation. *Proc. Natl. Acad. Sci. U.S.A.* **2022**, *119* (16), No. e2117716119.
(60) Chen, H.; Chen, K.; Huang, W.; Staudt, L. M.; Cyster, J. G.; Li, X. Structure of S1PR2-heterotrimeric G(13) signaling complex. *Sci. Adv.* **2022**, *8* (13), No. eabn0067.
(61) Liu, S.; Paknejad, N.; Zhu, L.; Kihara, Y.; Ray, M.; Chun, J.; Liu, W.; Hite, R. K.; Huang, X. Y. Differential activation mechanisms of lipid GPCRs by lysophosphatidic acid and sphingosine 1-phosphate. *Nat. Commun.* **2022**, *13* (1), 731.
(62) Akasaka, H.; Tanaka, T.; Sano, F. K.; Matsuzaki, Y.; Shihoya, W.; Nureki, O. Structure of the active G(i)-coupled human lysophosphatidic acid receptor 1 complexed with a potent agonist. *Nat. Commun.* **2022**, *13* (1), 5417.
(63) Navarro, G.; Gonzalez, A.; Sanchez-Morales, A.; Casajuana-Martin, N.; Gomez-Ventura, M.; Cordomi, A.; Busque, F.; Alibes, R.; Pardo, L.; Franco, R. Design of Negative and Positive Allosteric Modulators of the Cannabinoid CB2 Receptor Derived from the Natural Product Cannabidiol. *J. Med. Chem.* **2021**, *64* (13), 9354−9364.

https://doi.org/10.1021/acs.jcim.3c01054
J. Chem. Inf. Model. 2023, 63, 5927−5935